*Original Article*

SHM Structural Health Monitoring

*Structural Health Monitoring*
1–11

DOI: 10.1177/1475921716666532
shm.sagepub.com
SAGE

# Development of a "stick-and-detect" wireless sensor node for fatigue crack detection

**Peipei Liu[1], Hyung Jin Lim[1], Suyoung Yang[1], Hoon Sohn[1], Cheul Hee Lee[2], Yung Yi[3], Daewoo Kim[3], Jinhwan Jung[3] and In-hwan Bae[4]**

**Abstract**

A fatigue crack and its precursor often serves as a source of nonlinear mechanism for ultrasonic waves, and nonlinear ultrasonic techniques have been widely studied to detect fatigue crack at its very early stage. In this study, a wireless sensor node based on nonlinear ultrasonics is developed specifically for fatigue crack detection: (1) through packaged piezoelectric transducers, ultrasonic waves at two distinctive frequencies are generated, and their modulation due to a microcrack (less than 0.1 mm in width) is detected; (2) an autonomous reference-free crack detection algorithm is developed and embedded into the sensor node, so that users can simply "stick" the sensor to a target structure and automatically "detect" a fatigue crack without relying on any history data of the target structure; and (3) the whole design of the sensor node is fulfilled in a low-power working strategy. The performance of the sensor node is experimentally validated using aluminum plates with real fatigue cracks and compared with that of a conventional wired system. Furthermore, a field test in Yeongjong Grand Bridge in South Korea has been conducted with the developed sensor nodes.

**Keywords**

Structural health monitoring, wireless sensor node, fatigue crack, nonlinear ultrasonic modulation, reference-free damage detection

## Introduction

Civil and mechanical structures are susceptible to deterioration and damage during their service lifetime. Without proper nondestructive testing (NDT)/structural health monitoring (SHM) measures and subsequent corrective and preventive actions, the flaws in the aging or damaged structures will lead to catastrophic failures. Fatigue crack is estimated as the major flaw responsible for up to 90% of failures of in-service metallic structures.[1] Among various NDT/SHM techniques, ultrasonic testing has gained popularity in monitoring applications because those can benefit from built-in transduction and moderately large inspection ranges. However, for prevention of unexpected and sudden failure of metallic structures, it is of vital importance to detect the cracks in the early stage of the fatigue life, which the conventional linear ultrasonic techniques often fail to achieve. Studies have shown that the sensitivity of the nonlinear features created by cracks is far greater than what can be obtained from the conventional linear ultrasonic techniques.[2–8] The principal difference between them is that a small crack acts as an active radiation source of new frequency components in the nonlinear ultrasonic techniques rather than a passive scatter in the conventional linear techniques. This difference makes the nonlinear techniques a unique defect-sensitive instrument for detecting fatigue cracks.

Due to the crack-induced nonlinearity, ultrasonic wave can distort, create accompanying harmonics, multiply waves of different frequencies, and, under resonance conditions, change resonance frequencies as a function of driving amplitude. In undamaged

[1]Department of Civil & Environmental Engineering, KAIST, Daejeon, South Korea
[2]POTEC Co., Ltd., Daejeon, South Korea
[3]Department of Electrical Engineering, KAIST, Daejeon, South Korea
[4]New Airport Hiway Co., Ltd., Incheon, South Korea

**Corresponding author:**
Hoon Sohn, Department of Civil & Environmental Engineering, KAIST, Daejeon 34141, South Korea.
Email: hoonsohn@kaist.ac.kr

structures, these phenomena are weak, but remarkably large in damaged structures. There are two general nonlinear ultrasonic approaches for damage detection.[2] One approach, nonlinear resonant ultrasound spectroscopy, depends on the study of the nonlinear response of a single or a group of resonant modes within the structure. Resonance frequency shifts, harmonics, and damping characteristics are analyzed as function of the resonance peak acceleration amplitude.[3,4] The other approach is nonlinear ultrasonic modulation, which is based on nonlinear wave mixing in the structure. The manifestations of the nonlinear response appear as distortion and accompanying wave harmonics, and in sum and difference frequency generation (sidebands).[5–8] It has been reported that nonlinear techniques are robust to harmless factors like complicated geometry or moderate environmental variations like wind and temperature, and this robustness makes the nonlinear ultrasonic techniques quite suitable for field applications.[6]

As for data acquisition, conventional wired systems are bulky, difficult to apply for inaccessible areas, and demand an excessive amount of wires for monitoring of large-scale structures. To address these issues, much attention has been paid on distributed wireless sensor technology,[9] and many wireless sensors have been developed for temperature, strain, or impedance measurements,[10–12] with powerful computational cores included,[13] or to obtain low power consumption.[14,15] Meanwhile, some wireless sensors have been designed with actuation interfaces.[16,17]

The primary goal of this study is to develop a new kind of wireless sensor node which a user can simply stick to a target structure and start detecting fatigue crack. In comparison with the aforementioned literature, the uniqueness of this study lies in the following: (1) autonomous operation is realized in the developed wireless sensor node with a low-power working strategy, (2) microcrack (its width is in the level of μm) can be detected using nonlinear ultrasonic modulation technique, (3) no history data are required for structural damage diagnosis, (4) it is easy to extend to large-scale structure monitoring via wireless networking, and (5) the wireless sensor node is validated on a field bridge.

This article is organized as follows. Section "Development of a 'stick-and-detect' wireless sensor node" describes the development of the "stick-and-detect" wireless sensor node and the embedded autonomous crack detection algorithm. Section "Laboratory-scale validation using aluminum plates" presents the results of a laboratory-scale validation experiment and compares them with the results obtained from a conventional wired system. Section "Field test on Yeongjong Grand Bridge" showcases a field test performed on Yeongjong Grand Bridge. This article concludes with a brief summary and discussions in section "Summary and conclusion."

## Development of a "stick-and-detect" wireless sensor node

### Overview

An active "stick-and-detect" wireless sensor node is developed in this study for field applications in the future. We envision that once users stick the sensor nodes to the target structure, the sensor nodes will automatically form a wireless network and detect the onset of fatigue crack formation even without the history data obtained from the pristine condition of the structure.

The functional architecture of this sensor node is shown in Figure 1. The sensor node is composed of four major modules: excitation/sensing module, data acquisition/processing module, wireless communication module, and power supply module. The excitation/sensing module owns two excitation channels and one sensing channel for generating sinusoidal inputs at two distinctive frequencies and acquiring ultrasonic responses through packaged piezoelectric transducers (PZTs). PZTs are chosen because they can be easily mounted on the surface of the target structure. The data acquisition/processing module consists of a data logger, a processor, and an on-board memory. The data logger is in charge of controlling the excitation/sensing module, acquiring the ultrasonic response data and storing the data into the on-board memory. The processor in the data acquisition/processing module is for conducting signal processing with the developed autonomous crack detection algorithm. The wireless communication module takes charge of wireless network formation and wireless data transmission. Power supply module is responsible for providing uninterrupted power to the sensor node. The sensor node is designed to perform diagnosis periodically. It will wake up once every several weeks, and go back to sleep mode for minimizing the power consumption.

### Development of individual hardware components

Figure 2 shows the prototype of the "stick-and-detect" wireless sensor node. The packaged PZT shown in Figure 2(a) consists of three identical circular PZTs manufactured by APC International, and they are packaged by a Kapton tape with printed circuit and three SMA (SubMiniature version A) connecters. The diameter and the thickness of each PZT are 18 and 0.5 mm, respectively. Two of them are used for exerting sinusoidal inputs at two distinctive frequencies, and the

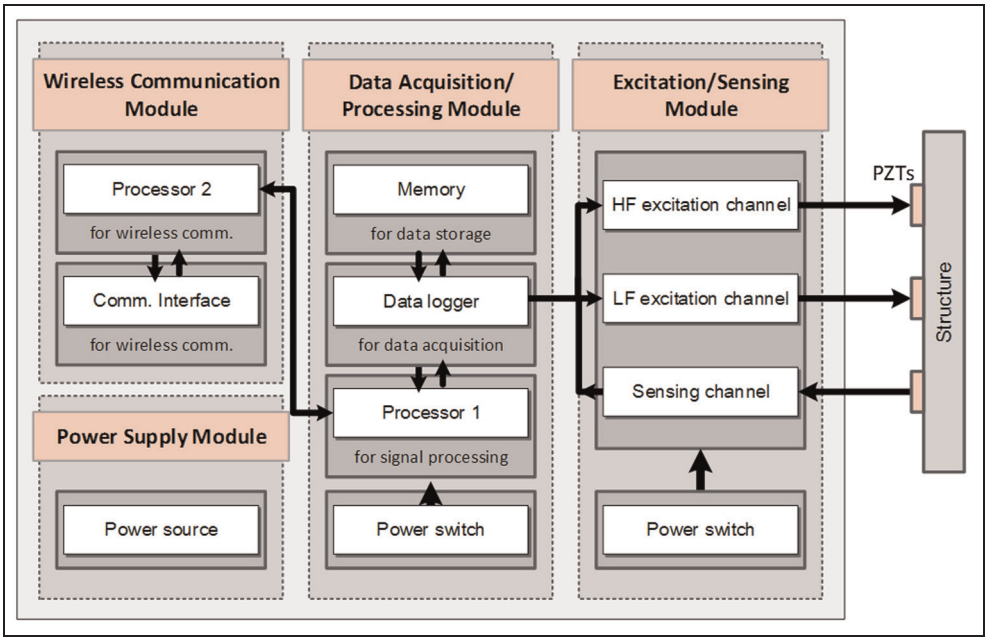


**Figure 1.** Functional architecture of the "stick-and-detect" wireless sensor node.

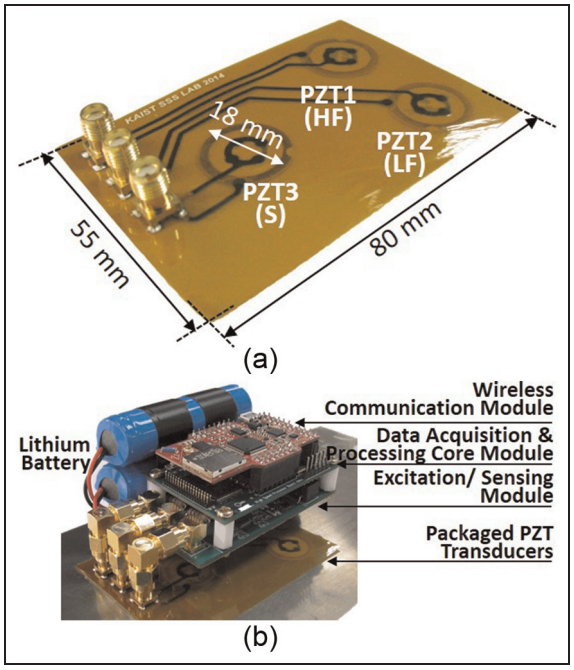


**Figure 2.** Prototype of the "stick-and-detect" wireless sensor node: (a) packaged PZT and (b) wireless sensor node.

third one is used for measuring the corresponding ultrasonic response. The packaged PZT is connected to the excitation/sensing module.

The excitation channel in the excitation/sensing module shown in Figure 3(a) consists of a serial 12-bit digital-to-analog converter (DAC), a direct current (DC) remover, a resistance–capacitance (RC) low-pass filter, and a power amplifier. The excitation channel can output a signal with a maximum peak-to-peak amplitude around 28 V and can excite a PZT ($C_{PZT} \leqslant 10$ nF) up to 200 kHz. The sensing channel in Figure 3(b) is composed of a charge amplifier, a high-pass filter, an anti-aliasing filter, a range/impedance matcher, and a serial 12-bit analog-to-digital converter (ADC). The charge amplifier converts the charge accumulated in PZT to a voltage signal. The sampling rate for the ADC is fixed at 1 MHz, along with an anti-aliasing filter at 300 kHz cutoff frequency. Low-frequency (LF) structural vibration and environmental noise below 2 kHz are removed using a Butterworth high-pass filter.

In the data acquisition/processing module, a field-programmable gate array (FPGA, EP4CE22E22C8) is chosen as the data logger for data acquisition. FPGA has no given processor structure but offers a large number of logic gates, resistors, static random-access memory (SRAM), and routing resources, which make it more flexible, and meets the lower power request. Also, since the FPGA is implemented with parallel computation, it achieves better and faster performance and is suitable as the data logger to acquire data from the excitation/sensing module. The acquired ultrasonic data are stored in the on-board memory (1 M × 16 SRAM). A microcontroller (32-bit ARM Cortex MCU, STM32F405RG) in this module is used for signal processing with the developed crack detection algorithm.

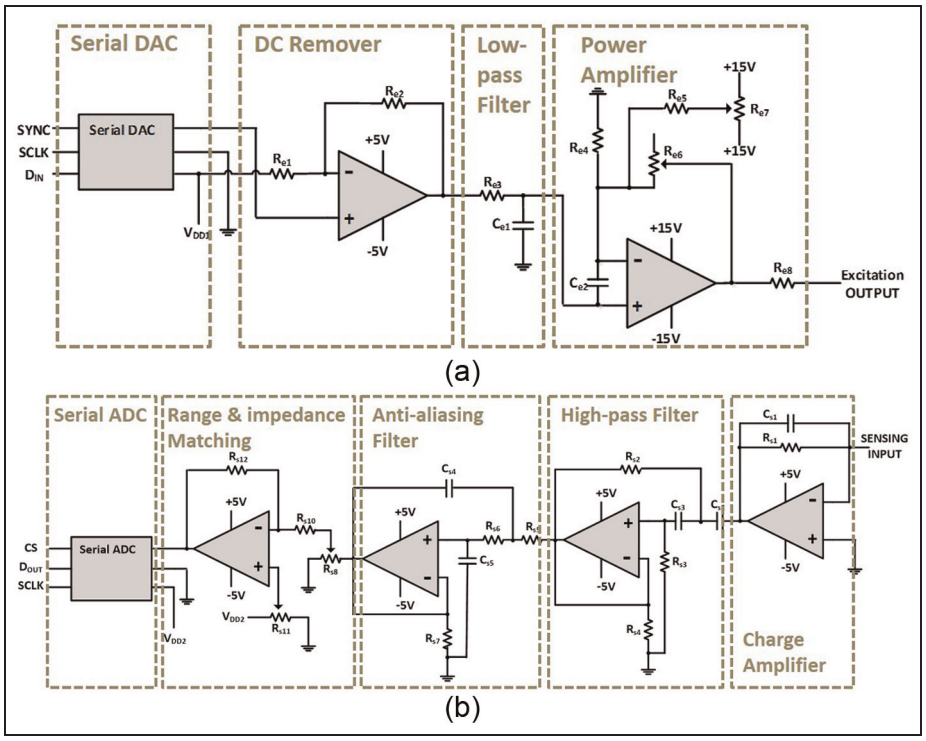


**Figure 3.** Schematic diagram of the excitation/sensing module: (a) excitation channel for signal generation and (b) sensing channel for response signal acquisition.

For the wireless communication module, a commercial Z1 module is adopted.[18] The Z1 module is composed of MSP430 processor and CC2420 communication interface (2.4-GHz IEEE 802.15.4 ZigBee compliant transceiver). Compared to conventional wireless personal area networks (WPANs), such as Bluetooth (IEEE 802.15.1) and radio-frequency identification (RFID), ZigBee has lower power consumption, higher data rate, and network reliability and supports three types of topology. The MSP430 processor is programmable for controlling the communication interface and sending out the diagnosis result.

For powering the sensor node, lithium battery is used at the present state. In addition, solar-based energy harvesting,[19,20] traffic-induced vibration energy,[21] and radio frequency (RF)-based wireless energy transmission[22] techniques are currently being explored as well. As for lowering the power requirement, a digital-controllable power switch is employed, so that the excitation/sensing module and the data acquisition/processing module can be completely shutdown with zero power request when they are in an idle state. The power switch is realized using a MOS FET Relay, which owns a low 20 mΩ on resistance and supports a continuous load current up to 2.5 A. The power switch for the excitation/sensing module is controlled by the FPGA in the data acquisition/processing module, while the power switch for the data acquisition/processing module is controlled by MSP430 in the wireless communication module.

For most of the time, the sensor node will be in an idle state, where the wireless communication module is at low-power sleep mode, and the other modules are all shut down by power switches. When the timer in MSP430 triggers, the sensor node wakes up and performs crack diagnosis. First, activated MSP430 turns on the power supply for the data acquisition/processing module and sends out structural damage diagnosis commands to it. Once the data acquisition/processing core module receives the commands, it turns on the power for the excitation/sensing module and starts the diagnosis procedure. All the modules in the sensor node will work together to acquire and process ultrasonic responses. Here, the power for the excitation/sensing module is turned off as soon as one batch of ultrasonic responses is received and turned on again for the next batch after the data acquisition/processing module finishes processing the first batch of the ultrasonic response. The on/off process continues until the last batch of the responses is obtained. Finally, the diagnosis is sent out to the end user, and the sensor node returns to the idle state, waiting for next timer trigger.

It is envisioned that the sensor node will wake up once every several weeks, perform crack detection, send out the diagnosis results, and go back to sleep. Since

**Table 1.** Power consumption of the sensor node.

| Module | Power consumption | |
|---|---|---|
| | Non-idle state (mW) | Idle state (μW) |
| Excitation/sensing module (with PZTs) | 1563.2 | 0 |
| Data acquisition/ processing module | 634.6 | 0 |
| Wireless communication module | 108.7 | 105.0 |

PZTs: piezoelectric transducers.

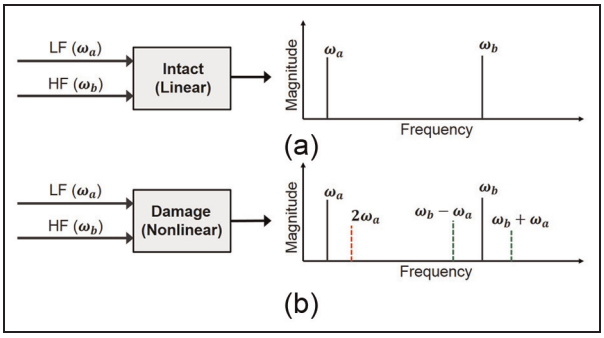


**Figure 4.** Illustration of nonlinear ultrasonic modulation when the structure is: (a) intact, and (b) damaged.

the sensor node will be mostly in the sleep mode, it is critical to reduce the power consumption during the idle state. That is, the power consumption of Z1 module during the idle state is the key factor for the overall power consumption. In the idle state, Z1 module falls into a sleep mode (low-power mode, LPM3 in MSP430) where it waits for an interruption from a low-power timer. In addition to this, we turn off all the other parts implemented in Z1 module such as on-board digital sensors and external memory. The power consumption for each module is tested and summarized in Table 1. In the idle state, the power consumption is just 105 μW, and the developed sensor node consumes only about 190.5 J in 3 weeks. Note that because the time lag between two consecutive wake-ups is around several weeks, PW-MAC (Predictive-Wakeup MAC), which is known as an energy-efficient protocol especially when data packets are generated with a long time lag,[23,24] is adopted to avoid excessive time drift among sensor nodes.

## *Development of an embedded autonomous crack detection algorithm*

When two inputs at two distinctive frequencies $\omega_a$ (LF) and $\omega_b$ (high frequency, HF) are applied to a linear system, since the nonlinear response is extremely small due to atomic nonlinearity and/or material nonlinearity, the response is supposed to contain the frequency components only at the input frequencies, as shown in Figure 4(a). However, if the structure is damaged, the manifestations of nonlinearity will become much clearer, for example, due to crack opening and closing, and the structural response will contain not only the input frequencies but also their harmonics (multiples of input frequencies) and modulations (linear combinations of input frequencies), as shown in Figure 4(b).[2] This phenomenon is called nonlinear ultrasonic modulation or nonlinear wave modulation.

As this phenomenon is originated from a nonlinear mechanism, it can be considered as a sign of nonlinearity presence or crack existence. However, it should be noted that the nonlinear ultrasonic modulation does not always occur even though crack exists in the structure. It occurs only if several binding conditions are satisfied, which can be briefly summarized as follows.[5,25,26] (1) Crack perturbation condition: the strain (displacement) at the crack location should be oscillated by both of the two inputs. In vibrations, this condition can be interpreted that nonlinear modulation components are not generated when the crack is located at the nodes of the vibration modes and (2) mode matching condition: the crack motion induced by one of the two inputs should modulate the other input at the crack location. Hence, the modulation generation significantly relies on the choice of two input frequencies and can be easily altered by crack configurations and even by environmental and operational conditions (e.g. temperature and loading) of the target structure.

Based on the nonlinear ultrasonic modulation technique and its binding conditions, an autonomous crack detection algorithm is developed and embedded into the sensor node. First, both sine LF and HF inputs are applied simultaneously to the structure, and the corresponding ultrasonic responses at $\omega_b \pm \omega_a (u_{\omega_b \pm \omega_a})$ are obtained using a modified discrete Fourier transform (DFT). Then, only HF inputs are applied $N$ times to get the ultrasonic noise responses $(n_{\omega_b \pm \omega_a, i},\ i = 1, 2, \ldots, N)$ at $\omega_b \pm \omega_a$. Here, $n_{\omega_b \pm \omega_a, i}$ is the sole outcome of the measurement noise because nonlinear modulation occurs only due to the interaction of HF and LF inputs. An exponential distribution is fitted to the population of $n_{\omega_b \pm \omega_a, i}$, and a threshold, $T_{\omega_b \pm \omega_a}$, corresponding to a user specified one-side confidence interval is obtained, respectively. The exponential distribution is chosen because the magnitude of the noise level is always positive in the frequency domain. This procedure is depicted in Figure 5, and the nonlinear index (NI) at $\omega_b \pm \omega_a$ is defined as

$$\mathrm{NI}_{\omega_b \pm \omega_a} = u_{\omega_b \pm \omega_a} - T_{\omega_b \pm \omega_a} \quad (1)$$

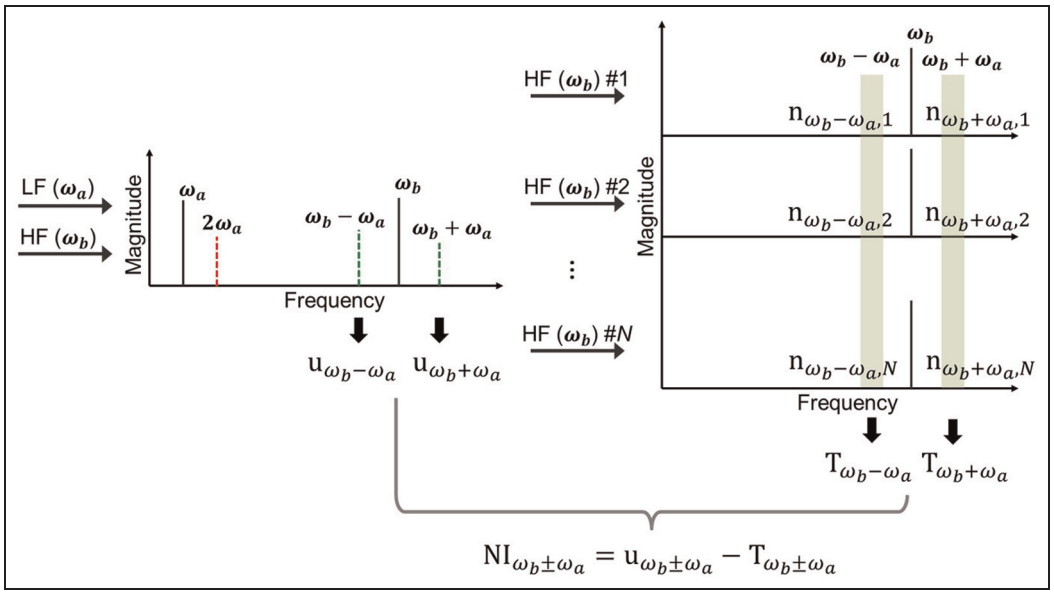


**Figure 5.** Nonlinear index (NI) extraction by comparing modulation (first sideband, $u_{\omega_b\pm\omega_a}$) and threshold value of noise ($T_{\omega_b\pm\omega_a}$).

Note that the $NI_{\omega_b\pm\omega_a}$ values will be mostly negative for an intact structure because the amplitude of $u_{\omega_b\pm\omega_a}$ is often below the noise threshold, $T_{\omega_b\pm\omega_a}$. On the other hand, $NI_{\omega_b\pm\omega_a}$ may show positive values when a fatigue crack exists, and the inputs ($\omega_a$ and $\omega_b$) satisfy the binding conditions. Considering that the binding conditions can be altered by crack configurations and even by environmental and operational conditions of the target structure, multiple NI values are obtained from different combinations of $\omega_a$ and $\omega_b$.

Based on the aforementioned observations, a fatigue crack is detected using "skewness" and "median" statistics of the NI values obtained from multiple combinations of $\omega_a$ and $\omega_b$. "Skewness" is the third standardized moment and defined is as

$$\text{Skewness} = E\left[\left(\frac{\text{NI} - \mu}{\sigma}\right)^3\right] \tag{2}$$

where $\mu$ and $\sigma$ are the mean and standard variation of the NI values, respectively, and $E$ is the expectation operator. The skewness represents the asymmetry of the distribution of the NI values. If a fatigue crack is formed, there will be more positive NI values, and the skewness is very likely to be positive. The median is the numerical value separating the higher half of a data sample from the lower half

$$\text{Median} = \frac{\left(\frac{M}{2}\right)^{\text{th}}\text{NI} + \left(\frac{M}{2}+1\right)^{\text{th}}\text{NI}}{2} \tag{3}$$

where $M$ is the total number (even number) of the NI values, and the NI values are arranged in the ascending order. Similarly, the median statistics of the NI values also has a high chance to be positive at the presence of the crack. Indeed, the skewness and median statistics are complementary to each other. The skewness statistics is effective in detecting a fatigue crack when the binding conditions are satisfied only at a few frequency combinations among all the investigated frequency combinations, and the nonlinear modulation occurs at a limited number of frequency combinations. On the other hand, the median statistics is useful when the nonlinear modulation occurs at the majority of the investigated frequency combinations. Therefore, the proposed autonomous crack detection is developed based on both statistics as follows: if both "skewness" and "median" statistics are negative, the structure is intact. Otherwise, a fatigue crack exists in the structure.

## Laboratory-scale validation using aluminum plates

### *Experimental setup*

The effectiveness of the developed sensor node is tested using the data obtained from two identical aluminum plate (6061 T6) specimens. The geometrical dimensions of the specimens are presented in Figure 6(a). Packaged PZTs, named PZT1, PZT2, and PZT3, are attached on each specimen. PZT1 and PZT2 are used for generating HF and LF signals, respectively, and PZT3 is for sensing. A 15-mm fatigue crack propagated from the center hole, as shown in Figure 6(b), is introduced to one specimen through a cyclic loading test. A universal testing machine (Instron 8801) with a 10 Hz cycle rate, a

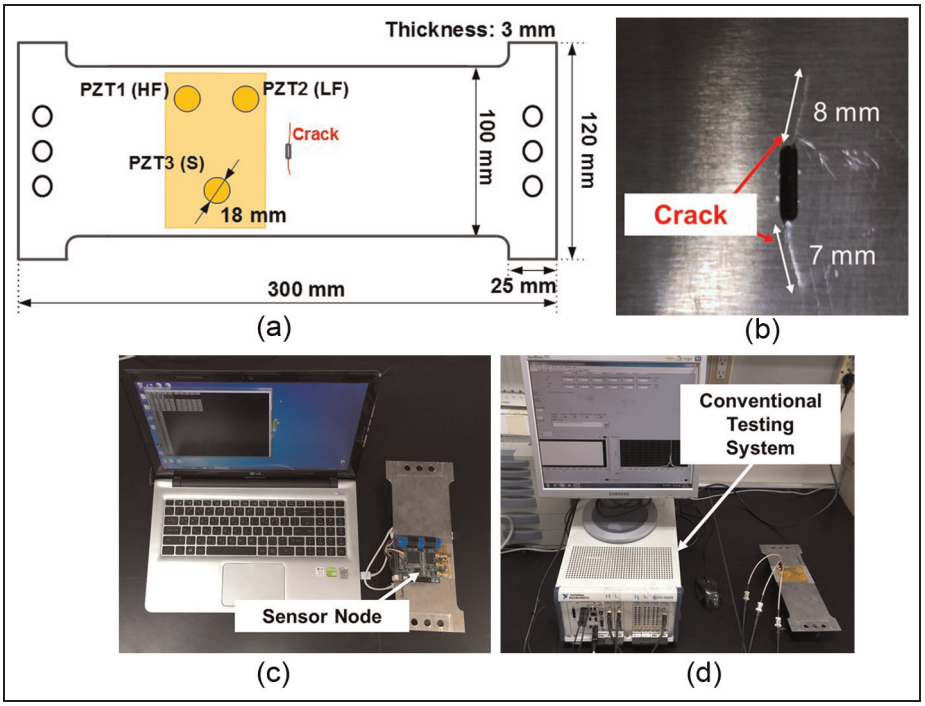


**Figure 6.** Experimental setup for laboratory-scale tests: (a) the geometry and dimensions of the specimen, (b) a close-up of the fatigue crack, (c) experimental setup with the developed sensor node, and (d) experimental setup with the conventional wired system.

maximum load of 25 kN, and a stress ratio of 0.1 is used for the cyclic loading test. The 15-mm fatigue crack is produced after 37,000 loading cycles, and its width is less than 20 μm. The packaged PZTs are connected to the wireless sensor node via SMA connectors (Figure 6(c)), and the sensor node is directly connected to a laptop computer. Here, the wireless communication module is not included in this test.

Meanwhile, the identical experiment is repeated using a conventional wired data acquisition system used in Lim et al.[6] for comparison (Figure 6(d)). The conventional wired system consists of two National Instruments' (NI) NI-PXI-5421 arbitrary waveform generators (AWGs) and a NI-PXI 5122 high-speed digitizer (DIG). One AWG is used to generate HF signal on PZT1 and the other to generate LF signal on PZT2. The response from PZT3 is measured by DIG. The AWGs and DIG are synchronized and controlled by LabVIEW software.

For both the sensor node and the conventional wired system, the output HF and LF signals are set with a peak-to-peak voltage of 20 V. The responses are measured with 1 MHz sampling rate for 0.25 s. The responses are measured four times and averaged in the time domain to improve the signal-to-noise ratio. For the combinations of LF and HF signals, $\omega_a$ is stepped from 40 to 50 kHz with a 1 kHz increment and $\omega_b$ is selected at 185 and 186 kHz. These LF and HF combinations are selected because the responses have relative large amplitudes at the corresponding input and modulations frequencies.

## *Experimental results for fatigue crack detection*

Figure 7(a) and (b) shows the NI values (arranged in the ascending order) obtained from the intact and damage aluminum plate specimens. The NI values are obtained using equation (1), and a threshold value corresponding to a 99.99% confidence interval is estimated by fitting an exponential distribution to four $n_{\omega_b \pm \omega_a, i}$ values. Since there are 22 different frequency combinations and 2 NI values are available at each frequency combination, a total of 44 NI values are obtained. The skewness and median statistics are calculated using all the 44 NI values.

Figure 7 demonstrates that both the skewness and median values are negative for the intact specimen, while the skewness value becomes positive for the damage specimen. Comparable results are obtained using the conventional wired system, as shown in Figure 8. Note that because the hardware specifications of the proposed sensor node and the conventional wired system are not exactly same, the ultrasonic modulation responses $u_{\omega_b \pm \omega_a}$, the noise values $n_{\omega_b \pm \omega_a, i}$, and the corresponded threshold $T_{\omega_b \pm \omega_a}$ obtained from two hardware systems are not identical. In spite of these

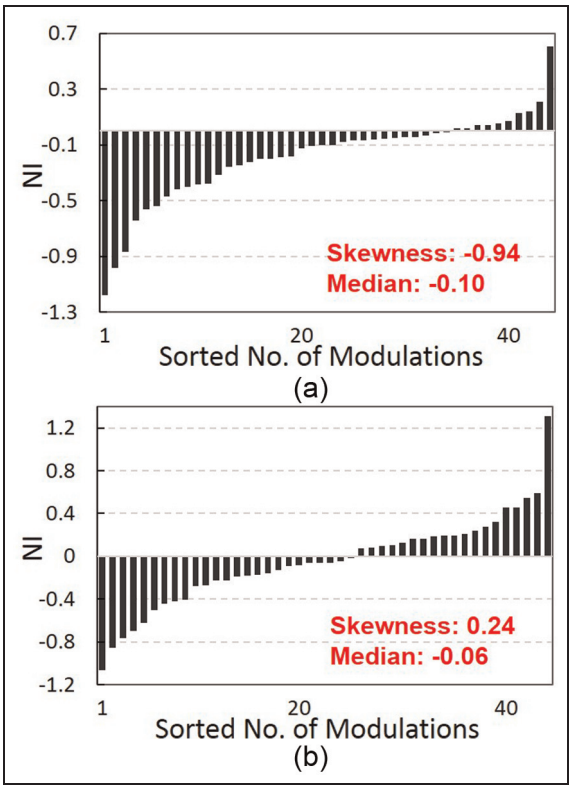


**Figure 7.** The skewness and median statistics of the NI values obtained from the developed sensor node: (a) data from the intact specimen and (b) data from the damage specimen.

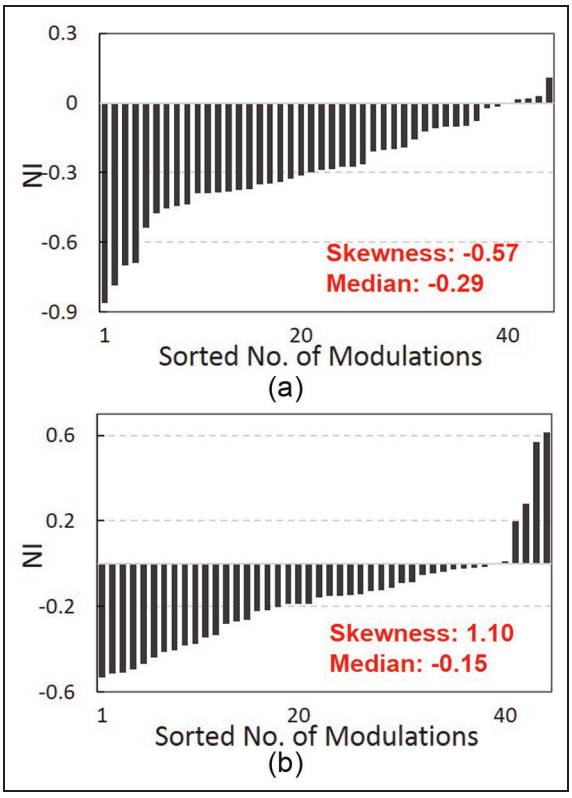


**Figure 8.** The skewness and median statistics of the NI values obtained from the conventional wired system: (a) data from the intact specimen and (b) data from the damage specimen.

differences, the fatigue crack in the aluminum plate specimen is successfully detected by both hardware systems.

## Field test on Yeongjong Grand Bridge

### *Field test setup*

The applicability of the developed wireless fatigue crack detection sensor to real in situ structures is tested by deploying the sensor nodes to Yeongjong Grand Bridge linking Yeongjong Island (Incheon Airport, ICN) and Incheon (Seoul) in South Korea (Figure 9(a)). This bridge completed in 2000 is the first three-dimensional (3D) self-anchored suspension bridge in the world and part of the Incheon International Airport Expressway. The total length of the bridge is 4420 m, of which the main suspension length and width are 550 and 35 m, respectively. The bridge carries both highway and railway, as shown in Figure 9(b). The double-deck system has six lanes of highways on the upper deck and four lanes of highways and two lanes of railways on the lower deck. The bridge is maintained by New Airport Hiway Co., Ltd., and around 400 sensors such as strain gauges, anemometers, and accelerometers are currently installed on the bridge.[27]

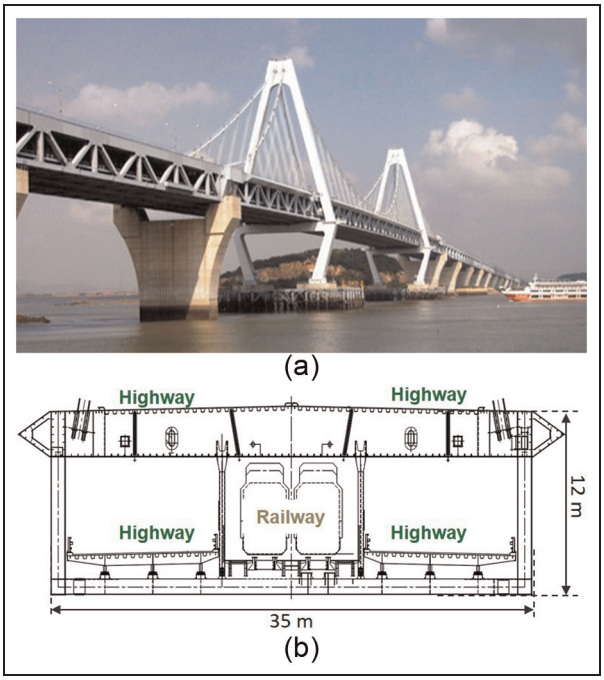


**Figure 9.** Yeongjong Grand Bridge: (a) overview of the bridge and (b) cross-sectional view of the bridge.

**Table 2.** Basic information of A'REX and KTX.

| Train | Operation | Length (no. of cars) | Weight without passengers |
|---|---|---|---|
| A'REX | Since 23 March 2007 | 117 m (6) | 203 t |
| KTX | Since 30 June 2014 | 388 m (20) | 692 t |

A'REX: Airport Railroad Express; KTX: Korean Train Express.

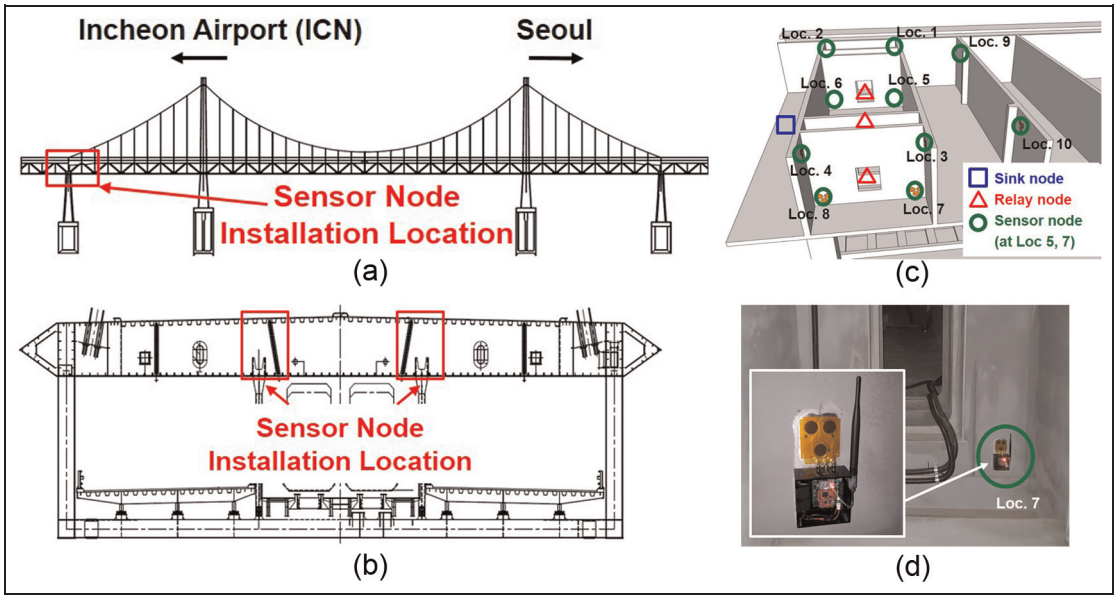


**Figure 10.** Sensor node installation on Yeongjong Grand Bridge: (a) side view, (b) cross-sectional view, (c) sensor locations inside the box girder of the upper deck, and (d) the wireless sensor node installed on location 7.

Before June 2005, only highway was carried on the bridge. Then, two lanes of railways were added, and Incheon Airport Railroad Express (A'REX) has been in operation since March 2007. From June 2014, Korean Train Express (KTX) also started to pass the bridge. One issue is that the length of KTX is 3 times longer and 3.5 times heavier than A'REX, as shown in Table 2. According to the data obtained from the instruments on the bridge, the maximum loading (the weight of locomotives) applied to the bridge is twice heavier than A'REX. Thus, application of proper monitoring systems is in urgent need for Yeongjong Grand Bridge.

The wireless sensor nodes are installed at the west end of the suspension section of Yeongjong Grand Bridge, as shown in Figure 10(a) and (b). A total of 10 wireless sensor nodes are installed near the welded connections inside the box girder of the upper deck where high stress level is expected due to train passage, as shown in Figure 10(c). These welded connections have been known to be prone to fatigue crack based on periodic visual inspections. Note that the optimal strategy is to install the sensor nodes close to the locations most susceptible to fatigue crack; otherwise, the detection sensitivity might be affected. Sensor data are transmitted from the sensor nodes to a sink node, as shown in Figure 10(c). Because the sensors are mostly placed inside enclosed spaces, three additional relay nodes are deployed. The relay nodes are capable of aggregating data packets from the sensor nodes within their clusters and transmitting them to the sink node via wireless multi-hop paths.[28] In this article, the sensor nodes placed on locations 5 and 7 (Figure 10(c)) are selected to show the field test results. Figure 10(d) shows the test site picture of location 7. All the test parameters are identical to the previous laboratory test unless described differently. $\omega_a$ is stepped from 40 to 50 kHz with a 1 kHz increment, and $\omega_b$ is selected at 197 and 198 kHz.

### *Field test results*

Figure 11(a) and (b) shows the NI values obtained from locations 5 and 7 (arranged in the ascending order). The NI values are computed by subtracting the modulation amplitude obtained at $\omega_b \pm \omega_a$ when LF and HF inputs are applied simultaneously from a threshold value. This threshold value corresponds to a

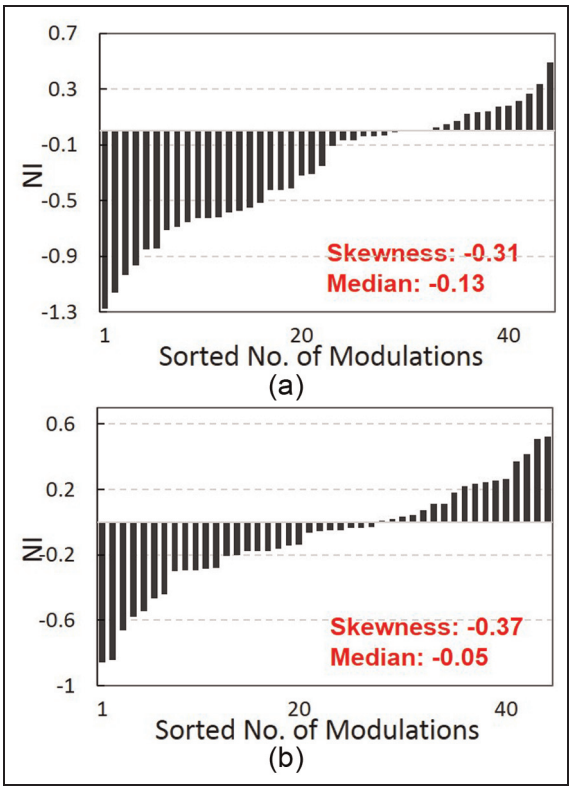


**Figure 11.** Fatigue crack detection results obtained from (a) location 5 and (b) location 7 shown in Figure 10(c).

99.99% confidence interval obtained by fitting an exponential distribution to four noise values at $\omega_b \pm \omega_a$ when only HF input is applied. A total of 44 NI values are obtained, and their skewness and median values are calculated to be negative both in locations 5 and 7. It is concluded that there is no fatigue crack near the inspected locations, and the diagnoses are confirmed by professional NDT engineers through visual inspection and magnetic penetrant inspection.

To check the robustness of the proposed crack detection algorithm and the sensor node, the identical test is repeated eight times, and their results are summarized in Table 3. The time interval between each test is around 1 h. The environmental and traffic conditions varied during the collection of the test data. For example, during the collection of some test data, KTX and A'REX passed through the bridge, while there were no trains for other cases. Although the skewness and median values slightly vary from one test to another, all the tests statistically remain negative, indicating that there are no major cracks in the monitored locations.

## Summary and conclusion

This study developed a "stick-and-detect" wireless sensor node for fatigue crack detection. Based on the nonlinear ultrasonic modulation technique, a reference-free crack detection algorithm is developed and implemented in this sensor node, so that fatigue crack can be detected at its early stage and without relying on any history data of the target structure. This sensor node is operated in a low-power working strategy taking advantage of digital-controllable power switches. All these make the developed sensor node own a potential for field applications. The performance of this sensor node is validated by comparing the fatigue crack detection results in an aluminum plate with the results obtained from a conventional wired system. Also, this sensor node is applied to Yeongjong Grand Bridge for field test. A follow-up study will focus on sensor node optimization and introduction of energy harvesting or wireless energy transmission techniques for power supply.

**Table 3.** Summary of field test results performed on Yeongjong Grand Bridge.

| Test no. | Location 5 | | Location 7 | |
|---|---|---|---|---|
| | Skewness | Median | Skewness | Median |
| 1 | −0.31 | −0.13 | −0.37 | −0.05 |
| 2 | −0.41 | −0.09 | −0.04 | −0.04 |
| 3 | −0.41 | −0.49 | −0.93 | −0.11 |
| 4 | −0.01 | −0.04 | −0.03 | −0.16 |
| 5 | −0.08 | −0.09 | −0.32 | −0.09 |
| 6 | −0.70 | −0.11 | −0.01 | −0.21 |
| 7 | −0.09 | −0.18 | −0.43 | −0.10 |
| 8 | −0.27 | −0.17 | −0.28 | −0.06 |

## Declaration of Conflicting Interests

The author(s) declared no potential conflicts of interest with respect to the research, authorship, and/or publication of this article.

## Funding

The author(s) disclosed receipt of the following financial support for the research, authorship, and/or publication of this article: This work was supported by the Smart IT Convergence System Research Center as Global Frontier Project (CISS-2012M3A6A6054195) funded by the Ministry of Education, Science and Technology (MEST) and a grant from Smart Civil Infrastructure Research Program (13SCIPA01) funded by Ministry of Land, Infrastructure and Transport (MOLIT) of Korea government.

## References

1. Campbell FC. *Elements of metallurgy and engineering alloys*. Cleveland, OH: ASM International, 2008.
2. Van Den Abeele KEA, Johnson PA and Sutin A. Nonlinear elastic wave spectroscopy (NEWS) techniques to

discern material damage, Part I: nonlinear wave modulation spectroscopy (NWMS). *Res Nondestruct Eval* 2000; 12: 17–30.
3. Van Den Abeele KEA, Carmeliet J, Ten Cate JA, et al. Nonlinear elastic wave spectroscopy (NEWS) techniques to discern material damage, part II: single-mode nonlinear resonance acoustic spectroscopy. *Res Nondestruct Eval* 2000; 12: 31–42.
4. Eiras JN, Kundu T, Bonilla M, et al. Nondestructive monitoring of ageing of alkali resistant glass fiber reinforced cement (GRC). *J Nondestr Eval* 2013; 32: 300–314.
5. Yoder NC and Adams DE. Vibro-acoustic modulation using a swept probing signal for robust crack detection. *Struct Health Monit* 2010; 9: 257–267.
6. Lim HJ, Sohn H, Desimio MP, et al. Reference-free fatigue crack detection using nonlinear ultrasonic modulation under changing temperature and loading conditions. *Mech Syst Signal Pr* 2014; 45: 468–478.
7. Dutta D, Sohn H, Harries KA, et al. A nonlinear acoustic technique for crack detection in metallic structures. *Struct Health Monit* 2009; 8: 251–262.
8. Klepka A, Staszewski WJ, Jenal RB, et al. Nonlinear acoustics for fatigue crack detection- experimental investigations of vibro-acoustic wave modulations. *Struct Health Monit* 2011; 11: 197–211.
9. Lynch JP and Loh KJ. A summary review of wireless sensors and sensor networks for structural health monitoring. *Shock Vib Digest* 2006; 38: 91–128.
10. Quinn W, Kelly G and Barrett J. Development of an embedded wireless sensing system for the monitoring of concrete. *Struct Health Monit* 2012; 11: 381–392.
11. Barroca N, Borges LM, Velez FJ, et al. Wireless sensor networks for temperature and humidity monitoring within concrete structures. *Constr Build Mater* 2013; 40: 1156–1166.
12. Chacón R, Guzmán F, Mirambell E, et al. Wireless sensor networks for strain monitoring during steel bridges launching. *Struct Health Monit* 2009; 8: 195–205.
13. Liu L and Yuan FG. Active damage localization for plate-like structures using wireless sensors and a distributed algorithm. *Smart Mater Struct* 2008; 17: 055022.
14. Torfs T, Sterken T, Brebels S, et al. Low power wireless sensor network for building monitoring. *IEEE Sens J* 2013; 13: 909–914.
15. Liu P, Yuan S and Qiu L. Development of a PZT-based wireless digital monitor for composite impact monitoring. *Smart Mater Struct* 2012; 21: 035018.
16. Zhao X, Qian T, Mei G, et al. Active health monitoring of an aircraft wing with an embedded piezoelectric sensor/actuator network: II. Wireless approaches. *Smart Mater Struct* 2007; 16: 1218–1225.
17. Lynch JP. Design of a wireless active sensing unit for localized structural health monitoring. *Struct Control Health Monit* 2005; 12: 405–423.
18. Low-power wireless module for IoT and WSN, http://zolertia.io/z1
19. Jang S, Jo H, Cho S, et al. Structural health monitoring of a cable-stayed bridge using smart sensor technology: deployment and evaluation. *Smart Struct Syst* 2010; 6: 439–459.
20. Min J, Park S, Yun CB, et al. Development of multifunctional wireless impedance sensor nodes for structural health monitoring. In: *Proceedings of the SPIE 7647 sensors and smart structures technologies for civil, mechanical, and aerospace systems*, San Diego, CA, 31 March 2010, 746728.
21. Galchev TV, McCullagh J, Peterson RL, et al. Harvesting traffic-induced vibrations for structural health monitoring of bridges. *J Micromech Microeng* 2011; 21: 104005.
22. Mascarenas DL, Flynn EB, Todd MD, et al. Experimental studies of using wireless energy transmission for powering embedded sensor nodes. *J Sound Vib* 2010; 329: 2421–2433.
23. Tang L, Sun T, Gurewitz O, et al. PW-MAC: an energy-efficient predictive-wakeup MAC protocol for wireless sensor networks. In: *Proceedings of the IEEE INFOCOM*, Shanghai, China, 10–15 April 2011, pp. 1305–1313. New York: IEEE.
24. Langendoen K and Meier A. Analyzing MAC protocols for low data-rate applications. *ACM T Sensor Network* 2010; 7: 19.
25. Lim HJ, Sohn H and Liu P. Binding conditions for nonlinear ultrasonic generation unifying wave propagation and vibration. *Appl Phys Lett* 2014; 104: 214103 (5 pp.).
26. Zaitsev VY, Matveev LA and Matveyev AL. On the ultimate sensitivity of nonlinear modulation method of crack detection. *NDT&E Int* 2009; 42: 622–629.
27. Oh CK, Sohn H and Bae IH. Statistical novelty detection within the Yeongjong suspension bridge under environmental and operational variations. *Smart Mater Struct* 2009; 18: 125022.
28. Tang J, Hao B and Sen A. Relay node placement in large scale wireless sensor networks. *Comput Commun* 2006; 29: 490–501.